Available online at www.sciencedirect.com
ScienceDirect
Bioorganic & Medicinal Chemistry 15 (2007) 7444–7458
Bioorganic & Medicinal Chemistry

Synthesis, antifungal and antimycobacterial activities of new bis-imidazole derivatives, and prediction of their binding to $P450_{14DM}$ by molecular docking and MM/PBSA method☆

Daniele Zampieri,[a] Maria Grazia Mamolo,[a,*] Luciano Vio,[a] Elena Banfi,[b] Giuditta Scialino,[b] Maurizio Fermeglia,[c] Marco Ferrone[c] and Sabrina Pricl[c]

[a]*Department of Pharmaceutical Sciences, Piazzale Europa 1, University of Trieste, 34127 Trieste, Italy*
[b]*Department of Biomedical Sciences, Microbiology Section, Via A. Fleming 32, University of Trieste, 34127 Trieste, Italy*
[c]*Department of Chemical, Environmental and Raw Materials Engineering, Piazzale Europa 1, University of Trieste, 34127 Trieste, Italy*

Received 6 February 2007; revised 12 June 2007; accepted 10 July 2007
Available online 22 August 2007

Abstract—New bis-imidazole derivatives have been synthesized and their antifungal and antimycobacterial activity was determined. Almost all compounds exhibited a moderate to good activity against two clinical isolates of *Candida albicans* 3038 and *Candida glabrata* 123. The same compounds showed an interesting killing activity against *Mycobacterium tuberculosis* $H_{37}Rv$ reference strain. Docking procedures combined with molecular dynamics simulations in the MM/PBSA framework of theory were applied to predict the binding mode of all compounds in the binding pocket of the cytochrome P450 14α-sterol demethylase (14DM) of *C. albicans*, for which no ligand–protein crystal structure is currently available. The results obtained in silico showed that the active compounds may interact at the active site of protein, and that their binding free energy values are in agreement with the corresponding experimental activity values.

1. Introduction

The increasing incidence of severe systemic mycoses frequently represents a significant cause of morbidity and mortality in immunocompromised patients, such as those affected by AIDS, cancer, or who received an organ transplant. Azoles are the most widely studied and currently used class of antifungal agents. However, the emergence of azole resistant strains has spurred the search for new antimycotic compounds. With the aim of obtaining new antifungal compounds, we synthesized the series of the bis-imidazole derivatives **1a**–**m** (Table 1). The in vitro activities of derivatives **1a**–**m** were tested against two clinical strains of *Candida albicans* 3038 and *Candida glabrata* 123, by comparing their minimal inhibiting concentrations (MICs) to those of two reference drugs, miconazole and amphotericin B, respectively.

The cytochrome P450-dependent lanosterol 14α-demethylase ($P450_{14DM}$, CYP51) is the target enzyme for azole antifungal agents in the ergosterol biosynthesis pathway. Azoles inhibit $P450_{14DM}$ causing accumulation of methylated sterols, depletion of ergosterol, and inhibition of cell growth. Because it was established, using genomic DNA from *Mycobacterium tuberculosis* (MT) $H_{37}Rv$ strain, that (i) a CYP-like gene encodes a bacterial sterol 14α-demethylase (MT $P450_{14DM}$)[1] which binds 14α-methyl sterols and azole inhibitors[2] of $P450_{14DM}$,[3,4] and (ii) many imidazole derivatives showed antimycobacterial activity associated with antifungal activity,[5–8] we tested compounds **1a**–**m** also for their possible antimycobacterial activity against a strain of *M. tuberculosis* $H_{37}Rv$. In this case, rifampicin was used as a reference compound.

This series of new inhibitors also offers a significant computational challenge to quantitatively evaluate the bind-

Keywords: Bis-imidazole; Antifungal and antimycobacterial activity; Docking; Free energy of binding.
☆ A preliminary account of this work was presented at Second Joint Italian–Swiss Meeting on Medicinal Chemistry, Modena, September 12–16, 2005.
* Corresponding author. Fax: +39 04052572; e-mail: mamolo@units.it

0968-0896/$ - see front matter © 2007 Elsevier Ltd. All rights reserved.
doi:10.1016/j.bmc.2007.07.023

Table 1. Yields and physical data of the synthesized compounds **1a–m**

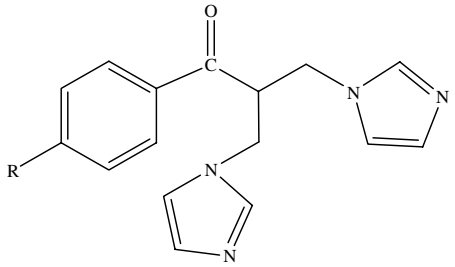

1 a-h

Compound	R	Mp (°C)	Yield (%)	Yield Microwave (%)	R_f ($CHCl_3$–EtOH) (8:2)	Anal. (C, H, N)	M_W
1a	H	212–5	10	32	0.18	$C_{16}H_{16}N_4O$	280.33
1b	Br	>270	11	50	0.20	$C_{16}H_{15}BrN_4O$	359.22
1c	Cl	>270	8	39	0.17	$C_{16}H_{15}ClN_4O$	314.77
1d	F	>270	7	44	0.20	$C_{16}H_{15}FN_4O$	298.32
1e	CH_3	240–2	13	42	0.25	$C_{17}H_{18}N_4O$	294.35
1f	OCH_3	222–4	36	69	0.38	$C_{17}H_{18}N_4O_2$	310.35
1g	NO_2	232–4	24	71	0.34	$C_{16}H_{15}N_5O_3$	325.35
1h	Ph	237–9	11	43	0.40	$C_{22}H_{20}N_4O$	356.43

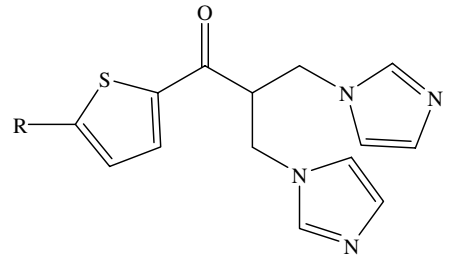

1 i-k

Compound	R	Mp (°C)	Yield (%)	Yield Microwave (%)	R_f ($CHCl_3$–EtOH) (8:2)	Anal. (C, H, N)	M_W
1i	H	258–60	18	55	0.25	$C_{14}H_{14}N_4OS$	286.36
1j	Br	>270	5	32	0.21	$C_{14}H_{13}BrN_4OS$	365.25
1k	Cl	249–51	9	36	0.20	$C_{14}H_{13}ClN_4OS$	320.80

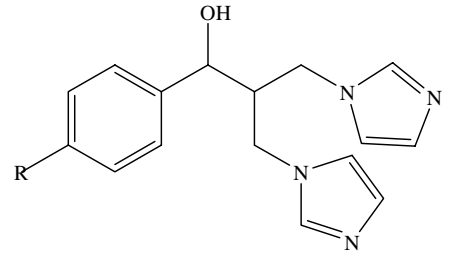

1 l-m

R	Compound	Yield (%)	Mp (°C)	R_f ($CHCl_3$–EtOH) (8:2)	Anal. (C, H, N)	M_W
4-Br	**1l**	30	180–2	0.26	$C_{16}H_{17}BrN_4O$	361.24
4-OCH_3	**1m**	36	155–7	0.23	$C_{17}H_{20}N_4O_2$	312.37

ing affinity to its target receptor. Although all molecules share a common scaffold, the substituents attached to the scaffold are quite diverse. Accordingly, in this work we calculate the free energy of binding of the synthesized inhibitors to cytochrome P450 14α-sterol demethylase (14DM) of *C. albicans* using the so-called Molecular Mechanics/Poisson–Boltzmann Surface Area (MM/PBSA) method.[9] This method is one of a class of approaches that attempts to include free energy terms directly into a molecular simulation. Basically, it combines explicit solvent molecular dynamics (MD) simulations with implicit solvation models, Poisson–Boltzmann (PB) analysis,[10] and solvent accessible surface area-dependent nonpolar solvation free energy calcula-

tions[11] to estimate free energies. A set of snapshots along the MD trajectory for each drug/enzyme complex are saved as representative conformations of the macromolecule/ligand system. The set of structures is then postprocessed with the explicit solvent replaced by a continuum solvent model. The free energy of the system then consists of the molecular mechanics potential energy of the complex, solvation free energy, and an entropy term for the complex. The solvation free energy, in turn, is composed of an electrostatic (or polar) portion, estimated by solving the PB equation, and a nonpolar solvation contribution, associated with the formation of a protein-sized cavity in the solvent, and van der Waals interactions between the complex and the solvent. Therefore, we have two further goals for this paper. First, we calculate free energies of association, relate these values to the corresponding experimental MIC, and provide insights into the interaction mechanism of the active site of $P450_{14DM}$ and the synthesized compounds. Second, we exploit all relevant information and explore modifications of these compounds that might result in a second-generation of new, more potent inhibitors.

2. Chemistry

1-Aryl-2-[(dialkylamino)methyl]-propenones can be prepared by Mannich reaction of the corresponding substituted acetophenones with paraformaldehyde and the corresponding secondary amines in acetic acid according to published procedures.[12a–c] Under these reaction conditions the intermediate 1-aryl-2-[(dimethylamino)methyl]-propenones **2a**–**h** and 2-[(dimethylamino)methyl]-1-(thiophene-2-yl)-propenones **2i**–**k** were prepared as hydrochlorides (Table 2) by treating the corresponding substituted arylmethylketones and thienylmethylketones with paraformaldehyde and dimethylamine hydrochloride in acetic acid. The 1-aryl-3-(1H-imidazol-1-yl)-2-[(1H-imidazol-1-yl)methyl]-propan-1-one derivatives **1a**–**h** and 3-(1H-imidazol-1-yl)-2-[(1H-imidazol-1-yl)methyl]-1-(thiophen-2-yl)-propan-1-one derivatives **1i**–**k** (Table 1) were prepared (Scheme 1) from propenone derivatives **2a**–**h** and **2i**–**k** by nucleophilic attack of imidazole both on carbon bearing the dimethylamino group and α,β-unsaturated ketone moiety via a Michael type reaction. Compounds were obtained in higher yields (Table 1) by microwave (MW) irradiation of the reagent mixture in EtOH–H_2O at room temperature. The optimal conditions were found to be 2 min of irradiation in open vials at 450 W for 5 times corresponding to a total time of 10 min. The conventional synthetic procedure required heating under reflux for reaction times varying from 12 to 36 h and, as already pointed out, the corresponding yields were quite lower (Table 1).

Table 2. Yields and physical data of the synthesized compounds **2a**–**k**

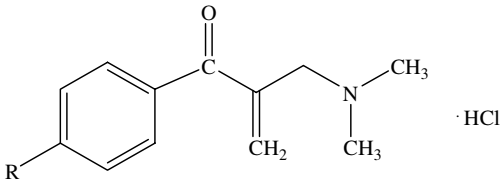

2 a-h

Compound	R	Mp (°C)	Yield (%)	R_f ($CHCl_3$–EtOH) (8:2)	Anal. (C, H, N)	M_W
2a[(a)12b]	H	156–9	48	0.18	$C_{12}H_{16}ClNO$	225.71
2b[(a)13]	Br	180–2	41	0.20	$C_{12}H_{15}BrClNO$	304.61
2c[(a)12b]	Cl	176–9	53	0.17	$C_{12}H_{15}Cl_2NO$	260.17
2d	F	170–2	47	0.20	$C_{12}H_{15}ClFNO$	243.71
2e[(a)13]	CH_3	140–2	55	0.25	$C_{13}H_{18}ClNO$	239.76
2f[(a)12b]	OCH_3	149–51	54	0.38	$C_{13}H_{18}ClNO_2$	255.75
2g	NO_2	200–02	65	0.34	$C_{12}H_{15}ClN_2O_3$	270.72
2h[(a)14]	Ph	182–4	62	0.40	$C_{18}H_{20}ClNO$	301.82

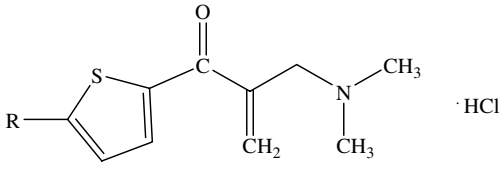

2 i-k

Compound	R	Yield (%)	Mp (°C)	R_f ($CHCl_3$–EtOH) (8:2)	Anal. (C, H, N)	M_W
2i	H	69	150–2	0.25	$C_{10}H_{14}ClNOS$	231.74
2j	Br	73	186–8	0.21	$C_{10}H_{13}BrClNOS$	310.64
2k	Cl	48	185–7	0.40	$C_{10}H_{13}Cl_2NOS$	266.19

[(a)]These compounds have been previously synthesized but not fully characterized on the basis of spectral data.

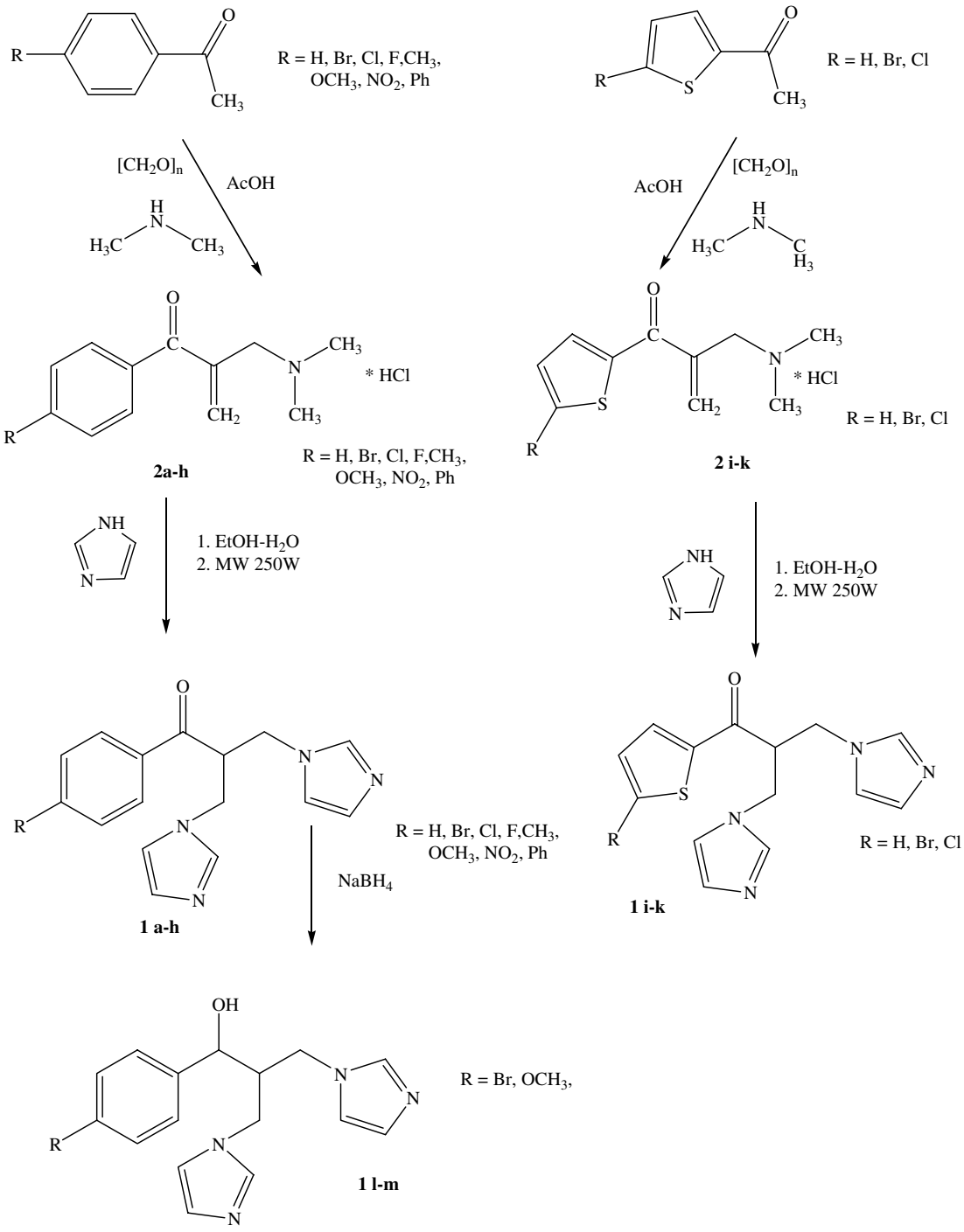

Scheme 1.

The reduction of the above obtained ketone derivatives **1 b** and **1f** with $NaBH_4$ produced the secondary alcohols **1l**,**m** (Table 1, Scheme 1).

3. Results and discussion

A series of bis-imidazole derivatives **1a**–**m** (Table 1) have been synthesized with the aim to evaluate their antifungal and antimycobacterial activities. The results of the in vitro evaluation of antifungal activity of compounds are reported in Table 3. The derivative **1h**, in which the biphenylyl moiety is present, exhibited a good inhibitory activity against the clinical strain of *C. albicans* 3038, with MIC values of 2 and 4 μg/mL after 24 h and 48 h, respectively. The activity was higher than that of the reference drug miconazole and similar to the activity of amphotericin B. The antifungal activity of the corresponding derivatives **1a**–**g** and **1i**–**k** against the strain of *C. albicans* 3038 was moderate, with MIC values ranging from 16 to 128 μg/mL and 32 to 128 μg/mL after 24 h and 48 h, respectively. The antifungal activities of compounds **1a**–**k** against the clinical strain of *C. glabrata* 123 were characterized by a similar profile,

Table 3. Activity of compounds **1a**–**m** against *Candida albicans* 3038, *Candida glabrata* 123, clinical strains and against *Mycobacterium tuberculosis* reference strain $H_{37}Rv$

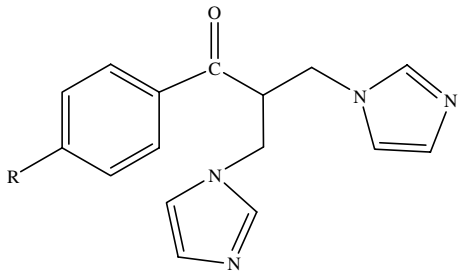

1 a-h

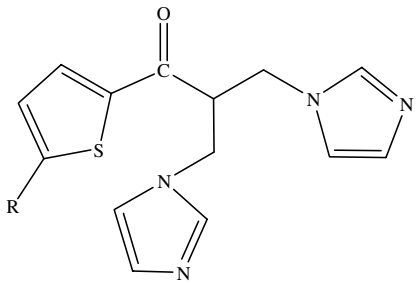

1 i-k

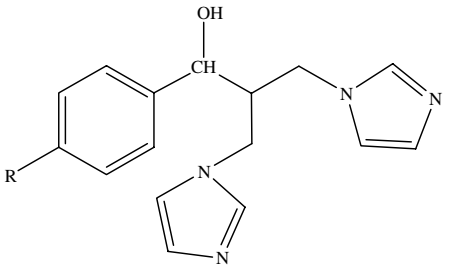

1 l-m

Compound	R	MIC (μg/mL)					Compound	R	MIC (μg/mL)					Compound	R	MIC (μg/mL)				
		C. albicans 3038		*C. glabrata* 123		*M. tuberc.* $H_{37}Rv$			*C. albicans* 3038		*C. glabrata* 123		*M. tuberc.* $H_{37}Rv$			*C. albicans* 3038		*C. glabrata* 123		*M. tuberc.* $H_{37}Rv$
		24 h	48 h	24 h	48 h				24 h	48 h	24 h	48 h				24 h	48 h	24 h	48 h	
1a	H	64	64	128	128	16	**2i**	H	128	128	128	128	16	**1l**	Br	128	>128	128	>128	8
1b	Br	16	32	32	64	16	**2j**	Br	64	64	64	128	16	**1m**	OCH_3	128	>128	128	>128	64
1c	Cl	16	32	32	64	16	**2k**	Cl	64	64	64	128	16							
1d	F	64	128	128	128	16														
1e	CH_3	64	128	128	128	8														
1f	OCH_3	64	128	128	128	16														
1g	NO_2	128	>128	128	>128	64														
1h	Ph	2	4	4	8	8														
Amphotericin B		1	2	0.5	2	Rifampicin	Amphoteric.B		1	2	0.5	2	Rifampicin	Amphoteric.B		1	2	0.5	2	Rifampicin
Miconazole		2.5	5	1.25	2.5	1 mg/disk	Miconazole		2.5	5	1.25	2.5	1 mg/disk	Miconazole		2.5	5	1.25	2.5	1 mg/disk

and only compound **1h** exhibited a remarkable antifungal activity against the tested strain, reaching MIC values of 4 μg/mL and 8 μg/mL after 24 h and 48 h, respectively. These MIC values were not very dissimilar from those of the reference drugs (Table 3).

Compounds **1l** and **1m**, with the hydroxylic function replacing the carbonyl group, were weakly active after 24 h, and devoid of antifungal activity on both *Candida* tested strains after 48 h. In summary, only compound **1h**, substituted with a phenyl group at position 4 of the benzene ring characterizing compounds **1a**–**h**, exhibited a considerable antifungal activity.

Compounds **1a**–**m** were also tested for antitubercular activity against the reference strain of *M. tuberculosis* $H_{37}Rv$, in comparison with rifampicin. The results of the in vitro antimycobacterial activity of compounds are reported in Table 3. All compounds exhibited a moderate activity, with MIC values in the range 8–64 μg/mL.

Accordingly to the results obtained for other imidazole derivatives [8,15–17] the newly synthesized imidazole derivatives showed both in vitro antifungal and antimycobacterial properties. Particularly, the antimycobacterial activity of compound **1h** was comparable to its antifungal activity towards the employed *Candida* strains, suggesting the presence of similar enzymatic interaction sites. To support this hypothesis, we performed a computational study of the molecular bases of the interactions between the synthesized compounds and the active site of the enzyme $P450_{14DM}$ with the additional, ultimate goal of exploiting this information in the design of further, more active inhibitors.

Generally speaking, there are two key requirements for the computer-aided structure-based drug design methods: (i) the generation of correct conformations of docked ligands, and (ii) the accurate prediction of binding affinity. To check whether our procedure complied with requirement (i), we modeled and docked fluconazole, for which the crystallographic structure in complex with 14DM of *M. tuberculosis* is available,[18] as a reference system. This was basically done by removing the inhibitor from the enzyme allosteric site, building a new molecular model for this compound, applying the conformational procedure described in details in Section 5 for the synthesized compounds, and finally docking it back into the protein binding pocket. The best docked structure, which is the configuration with the lowest docking energy in a prevailing cluster, was then compared with the corresponding crystal structure. Figure 1(a) and (b) shows a comparison between the co-crystallized conformation of fluconazole into the allosteric binding site of 14DM from *M. tuberculosis* and the docked conformation obtained upon application of the computational strategy adopted in this work.

At a first glance it can be seen that the agreement between the two structures is excellent: the root-mean-square deviation (RMSD) between the docked configuration and the relevant crystal structures of this test inhibitor is equal to 0.08 Å. In the light of these blank-test results, and of the fact that this computational ansatz was already successfully applied by us to predict the activity of allosteric inhibitors of HCV RNA-dependent RNA-polymerase,[19] and of other series of 14DM inhibitors,[8,20] the conceived modeling/docking procedure was applied for predicting the binding mode of the new compounds **1a**–**m** to 14DM of *C. albicans*.

The C_α RMSD of each complex from the docked structure for each MD simulation ranges from 0.48 to 1.09 Å. The all-atom RMSD of compounds **1a**–**m** in the complex from the initial docked models are in the range of 1–1.5 Å, which indicates that the initial conformations of these molecules generated according to the computational recipe described above are reasonable. Finally, the RMSD of the common inhibitor scaffold (–C–CH–$(CH_2$-imidazole$)_2$) is less than 1 Å. Accordingly, all these indications speak further in favor of the quality of the docking procedure adopted also for this set of new compounds (as well as for miconazole, see below).

One underlying assumption in our computational recipe is that both 14DM and its inhibitors undergo only a limited conformational change in going from the unbound to the bound state. The fluconazole blank-test reported and discussed above strongly supports this hypothesis. To verify the confined conformational changes of inhibitors **1a**–**m** upon binding to 14DM, however, we performed an MD simulation of **1h** in a box of water. In this case, we applied particle mesh Ewald summation[21] to treat long-range electrostatics, and with a 9 Å cutoff for the short-range nonbonded interactions. The simulation time was selected equal to the MM/PBSA production time, i.e. 400 ps. We verified that, during the MD run, the all-atom average RMSD is equal to 1.5 Å, as could be expected for molecules like these, characterized by a relatively rigid structure (see Fig. 2). Therefore, we think that our original assumption of minimal conformational change was utterly reasonable.

Interestingly, all compounds **1a**–**m** and miconazole were characterized by a similar docking mode in the active site of 14DM from *C. albicans* (see Fig. 3(a) and (b)). One of the two imidazole rings (1IR) of the inhibitors, and the corresponding moiety of miconazole, lies almost perpendicular to the heme group, with a ring nitrogen atom just above and coordinating the metal component of the prosthetic group.

The analysis of the MD trajectories reveals that the average dynamic distance (ADD) distance between N3(4) of the azole ring and the heme iron is 2.06 ± 0.5 Å, in good agreement with that found in the crystal structure of P450cam complexed with azole inhibitors.[22] Further stabilizing nonbonded interactions are established between the same azole ring (1IR) of each drug and the side chains of residues G254, M257, G258, and T262. The phenyl group of all compounds, as well as one of the aromatic moieties of miconazole, locate in a hydrophobic subsite above the prosthetic group. This subsite is delimited by the side chains of the ceiling residues F186, P187, and H261 on one side,

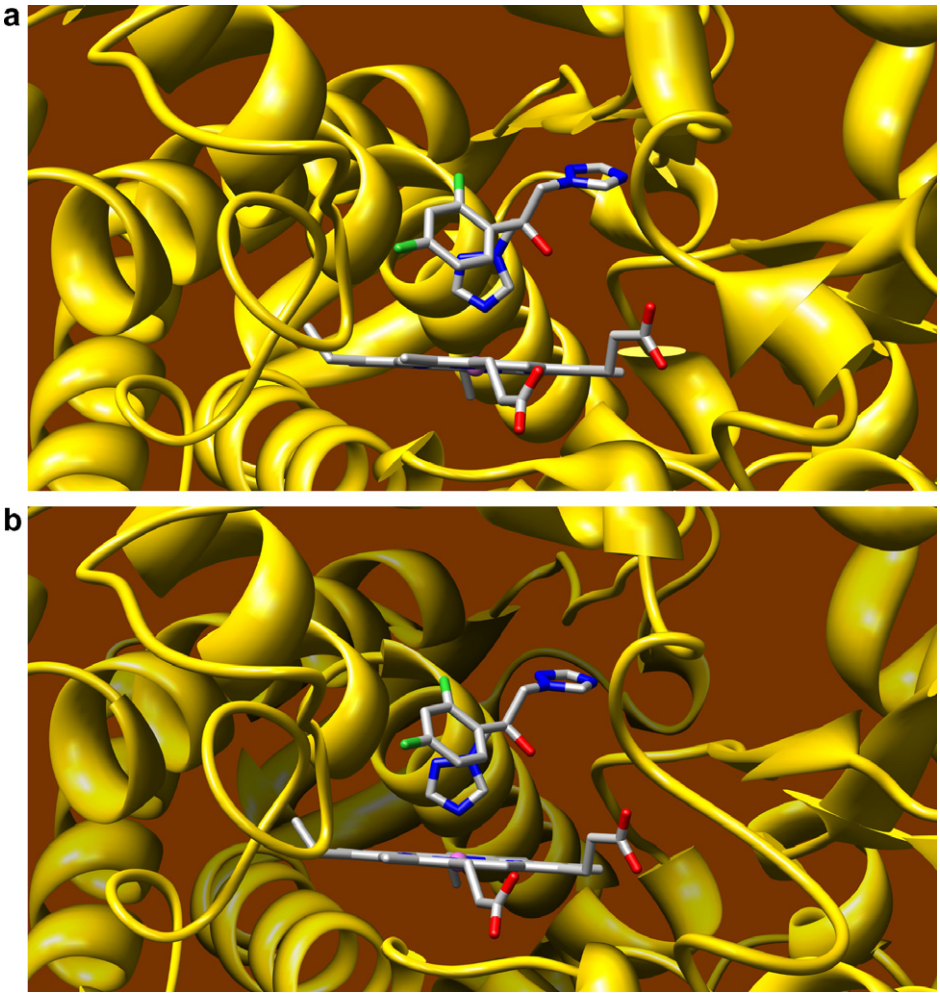

Figure 1. Comparison between the co-crystallized conformation of fluconazole into the active site of 14α-sterol demethylase from *Mycobacterium tuberculosis* (**a**), and the corresponding docked conformation of fluconazole in the same enzyme pocket obtained upon application of the computational strategy adopted in this work (**b**). The inhibitor molecules are shown as a stick model, and the atom color coding is as follows: carbon, gray; nitrogen, blue, oxygen, red; and chlorine, green. The heme group is also represented in sticks, with the iron ion depicted as a pink ball. Hydrogen atoms and water molecules are omitted for clarity.

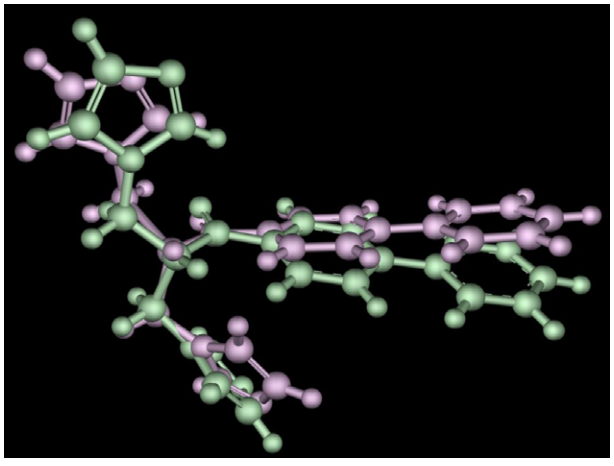

Figure 2. Superposition of the average structures of **1h** in water (pink) and in complex with 14DM (green).

and V460, V461, and L462 on the other. In an analogous fashion, the second imidazole ring (2IR), common to all inhibitors, and the halogenated phenyl ring of miconazole, are both stabilized by favorable dispersion forces with the side chains of K98, L354, V355, P357, and Y359. Interestingly, all structures of each 14DM/drug complex, as resulting from our validated docking/optimization procedure on similar enzyme/compound series,[8,20] did not predict any complex configuration featuring 2IR in coordination with the heme ion. We found that a sensible, neat reason for lies in the unfavorable steric reconfiguration the inhibitors must undergo to accommodate the CH_2-2IR moiety in a productive position in the active site (data not shown).

Finally, we verified that both the carbonyl (**1a**–**h** and **1i**–**k**) and hydroxyl oxygen atom (**1l**–**m**) of the synthesized compounds form a hydrogen bond with the –OH group of the T262 side chain, with an average dynamic distance of 2.82 Å.

Further insights and more quantitative information about the forces involved in substrate binding can be obtained by analyzing the values of the free energy of binding ΔG_{BIND} and its components, which are listed in Table 4 for the entire ligand family.

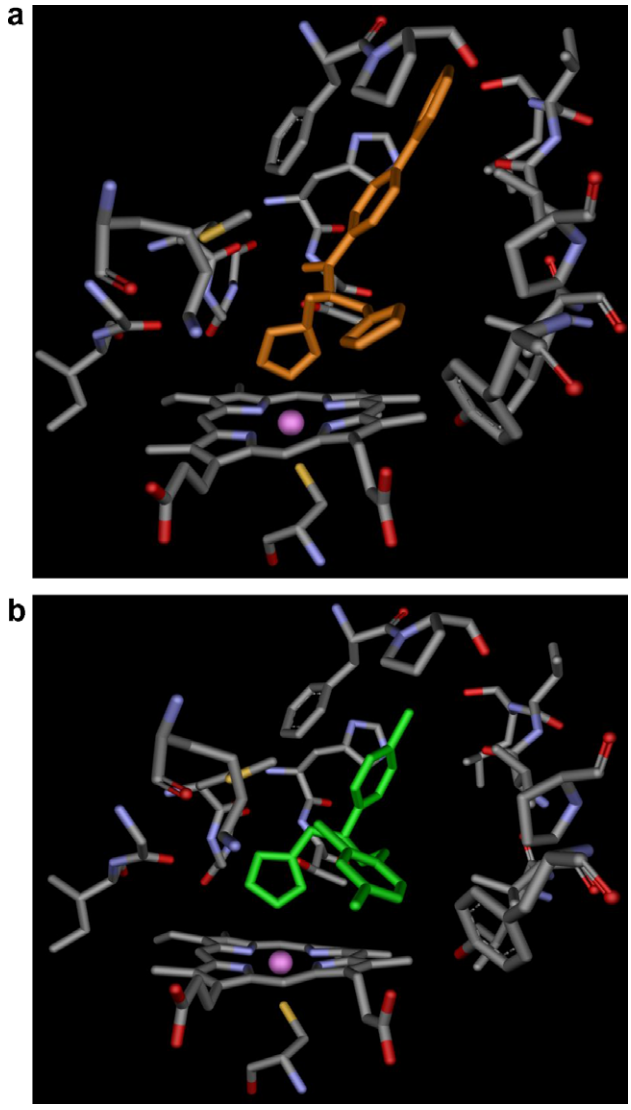

Figure 3. Equilibrated molecular dynamics snapshot of the docked compound **1h** (**a**), and the reference compound miconazole (**b**) in the active site of 14DM of *C. albicans*. The heme group and the amino acids pertaining to the binding site or contacting the ligands are shown in atom-colored sticks, and the ligands are in orange- (**1h**, (**a**)) and green-colored (miconazole, (**b**)) stick representation. Water molecules and hydrogen atoms are omitted for clarity.

As we can see from Table 4, both the intermolecular van der Waals and the electrostatics are important contributions to the binding. However, the electrostatic desolvation penalty ($\Delta G_{\mathrm{ELE}}^{\mathrm{SOLV}}$) offsets the favorable (i.e., negative) intermolecular electrostatics, yielding an unfavorable net electrostatic contribution to the compound affinities for the enzyme. As discussed above, the common molecular scaffold forms only a single, persistent hydrogen bond with the surrounding residues; the intermolecular electrostatic interactions are accordingly weak. Therefore, as previously verified for similar series of compounds,[8,20] the association between **1a**–**m** and cytochrome $P450_{14DM}$ is mainly driven by more favorable nonpolar interactions in the complex than in solution. This result was better evidenced by comparing the van der Waals/nonpolar ($\Delta E_{\mathrm{vDW}}^{\mathrm{MM}} + \Delta G_{\mathrm{NP}}^{\mathrm{SOLV}} = \Delta G_{\mathrm{APOL}}$) and ($\Delta E_{\mathrm{ELE}}^{\mathrm{MM}} + \Delta G_{\mathrm{ELE}}^{\mathrm{SOLV}} = \Delta G_{\mathrm{POL}}$) contribution for all molecules reported in Table 4. The ΔG_{APOL} contributions to ΔG_{BIND} for the **1i**–**k**/14DM complexes are less favorable (from 3 to 6 kcal/mole) than for the remaining complexes, because of a less negative van der Waals term. The analysis of the MD trajectories and the relevant 3D models reveals that the presence of the thiophene ring induces a non-optimal sterical configuration of the global molecules for binding, ultimately resulting in the lowest energy contributions of both electrostatic and van der Waals terms ΔG_{BIND}. Interestingly, however, the desolvation penalties upon binding of these inhibitors are also lower. Thereby, the net electrostatic contributions to 14 DM binding for **1i**–**k** are not significantly unfavorable, and their ΔG_{BIND} values are comparable to those of the other molecules of this series.

Compound **1h** (see Fig. 3(a)) exhibits the highest affinity toward 14DM of *C. albicans*, with $\Delta G_{\mathrm{BIND}} = -7.36$ kcal/mol. Besides the several van der Waals and hydrophobic interactions this molecule can form with the residues making up the enzyme binding site, common to all inhibitors, Figure 3(a) reveals a further, important π–π stabilizing interaction occurring between both aromatic rings of **1h** and the phenyl side chain of F186, resulting from the parallel-displaced geometry of these residues. The electronic nature of the π–π interactions indeed favors the stacking of aromatic rings either by parallel-displaced (off-center) or edge-on (T-stacking) geometries, while the face-to-face geometry is unfavorable (particularly in environments where there is a low effective dielectric constant), since the dominant interaction is π-electron repulsion. The average dynamic distances of the F186 aromatic ring from the two phenyl substituents of **1h** are 3.7 Å for the aromatic moiety directly linked to the scaffold and 4.7 Å for the aromatic ring as a substituent in **1h** only, respectively.

Finally, although we cannot directly correlate the calculated binding energies to the experimental MIC values, the trend exhibited by our ΔG_{BIND} values and the MIC is in good agreement, with a correlation coefficient equal to 0.92. Importantly, the calculated free energy for miconazole confirms that this reference drug is the tighter binder of 14DM as expected.

These results allowed us to be confident that the techniques and procedures adopted in this work for docking compounds **1a**–**m** to the active site of 14DM, and estimating their free energy of binding, were accurate enough to be used in a multistep virtual screening protocol. Under this perspective, we used the PROFEC suite of programs[23] to study how the most active inhibitor of this series, **1h**, could be modified to further improve its binding affinity toward 14DM. PROFEC is a set of software tools for carrying out and displaying extrapolative free energy calculations. Specifically, the PROFEC software suite calculates the free energy for inserting a specified test particle at a grid of points near the ligand of interest. A weighted electrostatic potential is also calculated for each position on this grid. These two (van der Waals and electrostatic) grids can be visualized and overlaid on a three-dimensional structure of

Table 4. Free energy components and total binding free energies for compounds **1a**–**m**

Compound	ΔE_{ELE}^{MM}	ΔE_{vDW}^{MM}	ΔE_{MM}	ΔG_{ELE}^{SOLV}	ΔG_{NP}^{SOLV}	ΔG_{SOLV}	$T\Delta S$	ΔG_{BIND}
1a	−34.48	−32.01	−66.49	49.45	−3.53	45.92	14.67	−5.90
1b	−35.98	−32.64	−68.62	51.71	−3.25	48.46	14.06	−6.10
1c	−36.41	−33.11	−69.52	53.43	−3.19	50.24	12.74	−6.54
1d	−36.06	−33.00	−69.06	52.65	−3.57	49.08	13.98	−6.00
1e	−34.01	−31.05	−65.06	49.56	−3.31	46.25	13.09	−5.72
1f	−35.02	−32.17	−67.19	52.44	−3.47	48.97	12.56	−5.66
1g	−36.49	−30.91	−67.40	53.65	−3.57	50.08	13.01	−4.31
1h	−35.87	−34.01	−69.88	50.93	−3.18	47.75	14.77	−7.36
1i	−31.18	−27.51	−58.69	43.05	−3.54	39.51	14.72	−4.46
1j	−31.72	−28.54	−60.26	44.77	−3.21	41.56	13.31	−5.39
1k	−31.51	−28.17	−59.68	44.01	−3.44	40.57	13.84	−5.27
1l	−36.99	−31.06	−68.05	53.72	−3.15	50.57	13.45	−4.03
1m	−36.06	−31.59	−67.65	53.91	−3.24	50.67	12.78	−4.20
Miconazole	−42.45	−47.18	−89.63	68.31	−3.45	64.86	14.89	−9.88

All energies are in kcal/mol.

the ligand or ligand–receptor complex to suggest positions where modifications to the ligand would improve binding. The main strengths of PROFEC are its unbiased evaluation of possible modifications and the ability to explicitly include the effect of solvation in the analysis. By postprocessing the MD trajectories of **1h** in solution and in complex with 14MD, PROFEC estimated the free energy cost of adding a test group to the inhibitor. One of the most interesting modifications resulting from running PROFEC is in the para and one ortho positions of the phenyl ring substituent of **1h**, as shown in Figure 4(a).

As suggested by PROFEC analysis, both *p*-H and *o*-H should be replaced with two hydroxyl groups: in fact, as seen in Figure 4(b), the new *p*-OH group can potentially form a hydrogen bond with the nitrogen atom of the peptidic bond between V461 and L462, whilst the *o*-OH will eventually be stabilized by a bifurcated H-bond with the carbonyl oxygen of the CONH moiety linking P187 and N188, and with the CO of the aminoacidic bond between again P187 and F186, respectively. Therefore, by applying the RESP fitting scheme,[24] we kept all charges of the inhibitor fixed except for the two, new modified groups. Next, we carried out a new molecular dynamics simulation of the new designed compound **1n** in complex with 14DM by applying the same computational protocol described above. Table 5 lists the free energy of binding for **1n**.

It is well evident that, when *p*-H and *o*-H are replaced by two –OH groups, both the intermolecular van der Waals and electrostatic interactions become more favorable, although, as expected from the introduction of two polar groups, more desolvation penalty has to be paid. Accordingly, the increase in favorable ΔE_{ELE}^{MM} with respect to **1h** (2.47 kcal/mol, see Tables 4 and 5) is more than cancelled out by the unfavorable ΔG_{ELE}^{SOLV} (5.70 kcal/mol); on the other hand, ΔE_{vDW}^{MM} is increased favorably by 4.31 kcal/mol. Overall, however, the binding free energy is improved by 1.42 kcal/mol; therefore, as a result of the PROFEC calculations, it seems that the –OH substitutions at the *p*-H and *o*-H positions of **1h** ought to yield a tighter binder and, hence, a stronger inhibitor of 14DM.

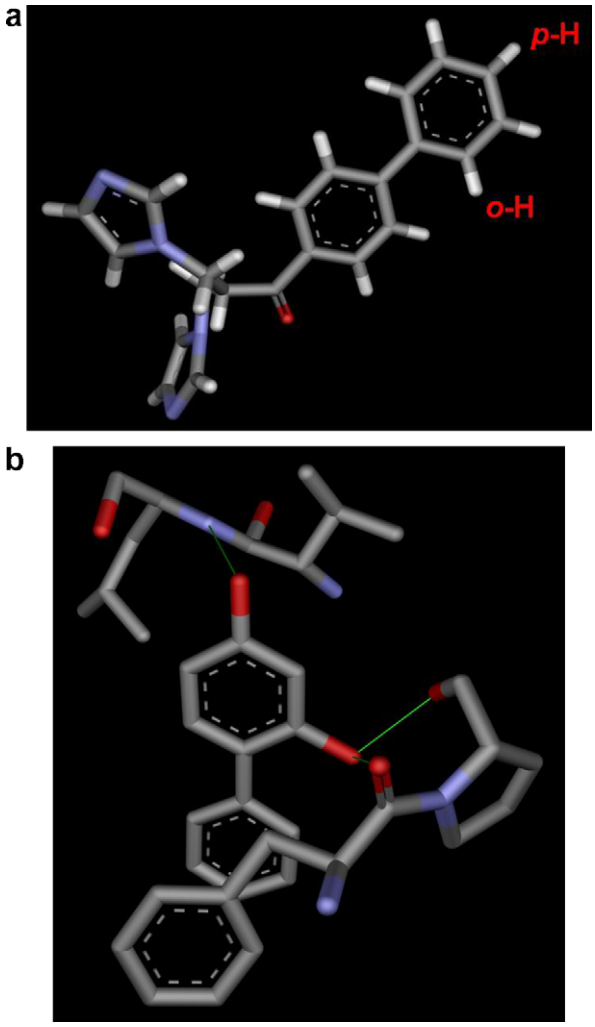

Figure 4. (**a**) Model of compound **1h** showing the potential sites for modification as suggested by PROFEC. (**b**) Details of compound **1n** resulting from design according to PROFEC indications (see text for details). The new, potential hydrogen bonds are represented by green lines.

Table 5. Free energy components and total binding free energies for compound **1n**

Compound	ΔE_{ELE}^{MM}	ΔE_{vDW}^{MM}	ΔE_{MM}	ΔG_{ELE}^{SOLV}	ΔG_{NP}^{SOLV}	ΔG_{SOLV}	$T\Delta S$	ΔG_{BIND}
1n	−38.34	−38.32	−76.66	56.63	−3.56	53.07	14.81	−8.78

All energies are in kcal/mol.

4. Conclusions

Almost all synthesized bis-imidazole derivatives described for the first time in this work exhibited some degree of antifungal and antimycobacterial activity, compound **1h** being the most active antifungal derivative in the series. The application of combined docking/MM-PBSA free energy of binding calculations allowed us to rationalize the interactions between the two series of inhibitors and the active site of the 14DM both from a qualitative and, most importantly, from a quantitative point of view. Particularly in the last case, we verified an agreement between the calculated ΔG_{BIND} values of all compounds and the correspondent experimental evidences, expressed in terms of MIC. Accordingly, the models and procedures proposed will be used in our laboratories for targeted computer-assisted drug design and subsequent prediction of activity of the new, potential inhibitors in reasonable length of computer and human time.

5. Experimental

Melting points were determined with a Buchi 510 capillary apparatus and are uncorrected. Infrared spectra in Nujol mulls were recorded on a Jasco FT 200 spectrophotometer. Proton nuclear magnetic resonance (^{1}H NMR) spectra were determined on a Varian Gemini 200 spectrometer, chemical shifts are reported as δ (ppm) in DMSO-d_6 solution. Reaction courses and product mixtures were routinely monitored by thin-layer chromatography (TLC) on silica gel precoated F_{254} Merck plates. ESI-MS spectra were obtained on a PE-API I spectrometer by infusion of a solution of the sample in MeOH. Elemental analyses (C, H, N) were performed on a Carlo Erba analyzer and were within ±0.3 of the theoretical value.

5.1. Synthesis

5.1.1. General method for synthesis of compounds 2a–k

5.1.1.1. 2-[(Dimethylamino)methyl]-1-phenyl-propenone hydrochloride (2a). To a solution (3.0 g, 25 mmol) of acetophenone in 50 ml of acetic acid, 1.5 g (50 mmol) of paraformaldehyde and 2.0 g (25 mmol) of dimethylamine hydrochloride were added. The mixture was heated under stirring for 16 h. Thereafter, the solvent was removed under reduced pressure. To remaining oil 70 ml of acetone was added and the formed precipitate was filtered to give 2.73 g (48%) of the chromatographically pure compound **2a**. Mp 156–159 °C. R_f = 0.37 ($CHCl_3$–EtOH 9:1). IR (Nujol, cm^{-1}): 1780. ^{1}H NMR (DMSO-d_6): 2.76 (s, 6H, $(CH_2)_3N$), 4.12 (s, 2H, CH_2), 6.18 (s, 1H, $=CH_2$), 6.81 (s, 1H, $=CH_2$), 7.50–7.85 (m, 5H, arom.), 11.20 (br s, 1H, NH^+ disappearing in D_2O). Anal. ($C_{12}H_{16}ClNO$) C, H, N: C calcd 63.85; found 63.72; H calcd, 7.14; found 7.21; N calcd, 6.21%; found 6.33.

Compounds **2b–k** were obtained similarly. Yields and melting points are reported in Table 2.

5.1.1.2. 1-(4-Bromophenyl)-2-[(dimethylamino)methyl]-1-propenone hydrochloride (2b). IR (Nujol, cm^{-1}): 1788. ^{1}H NMR (DMSO-d_6): 2.75 (s, 6H, $(CH_2)_3N$), 4.07 (s, 2H, CH_2), 6.19(s, 1H, $=CH_2$), 6.78 (s, 1H, $=CH_2$), 7.67–7.81 (m, 4H, arom.), 11.07 (br s, 1H, NH^+ disappearing in D_2O). Anal. ($C_{12}H_{15}BrClNO$) C, H, N: C calcd 47.32, found 47.53; H calcd, 4.96, found 5.10; N calcd, 4.60, found 4.48.

5.1.1.3. 1-(4-Chlorophenyl)-2-[(dimethylamino)methyl]-1-propenone hydrochloride (2c). IR (Nujol, cm^{-1}): 1783. ^{1}H NMR (DMSO-d_6): 2.77 (s, 6H, $(CH_2)_3N$), 4.10 (s, 2H, CH_2), 6.20 (s, 1H, $=CH_2$), 6.80 (s, 1H, $=CH_2$), 7.62 (d, 2H, arom., J = 8.54 Hz), 7.82 (d, 2H, arom., J = 8.54 Hz), 11.15 (br s, 1H, NH^+ disappearing in D_2O). Anal. ($C_{12}H_{15}Cl_2NO$) C, H, N: C calcd 55.40, found 55.62; H calcd, 5.81, found 5.93; N calcd, 5.38, found 5.22.

5.1.1.4. 2-[(Dimethylamino)methyl]-1-(4-fluorophenyl)-propenone hydrochloride (2d). IR (Nujol, cm^{-1}): 1785. ^{1}H NMR (DMSO-d_6): 2.78 (s, 6H, $(CH_2)_3N$), 4.10 (s, 2H, CH_2), 6.19 (s, 1H, $=CH_2$), 6.77 (s, 1H, $=CH_2$), 7.40–7.90 (m, 4H, arom.), 11.06 (br s, 1H, NH^+ disappearing in D_2O). Anal. ($C_{12}H_{15}ClFNO$) C, H, N: C calcd 59.14, found 59.28; H calcd, 6.20, found 6.27; N calcd, 5.75, found 5.68.

5.1.1.5. 2-[(Dimethylamino)methyl]-1-(4-methylphenyl)-propenone hydrochloride (2e). IR (Nujol, cm^{-1}): 1788. ^{1}H NMR (DMSO-d_6): 2.41 (s, 3H, CH_3), 2.77 (s, 6H, $(CH_2)_3N$), 4.10 (s, 2H, CH_2), 6.16 (s, 1H, $=CH_2$), 6.73 (s, 1H, $=CH_2$), 7.37 (d, 2H, arom., J = 7.93 Hz), 7.73 (d, 2H, arom., J = 7.93 Hz), 10.90 (br s, 1H, NH^+ disappearing in D_2O). Anal. ($C_{13}H_{18}ClNO$) C, H, N: C calcd 65.13, found 65.22; H calcd, 7.57, found 7.61; N calcd, 5.84, found 5.80.

5.1.1.6. 2-[(Dimethylamino)methyl]-1-(4-methoxyphenyl)-propenone hydrochloride (2f). IR (Nujol, cm^{-1}): 1783. ^{1}H NMR (DMSO-d_6): 2.81 (s, 6H, $(CH_2)_3N$), 3.80 (s, 3H, OCH_3), 3.91 (s, 2H, CH_2), 6.15(s, 1H, $=CH_2$), 6.70 (s, 1H, $=CH_2$), 7.18 (d, 2H, arom., J = 8.79 Hz), 8.20 (d, 2H, arom., J = 8.79 Hz), 11.30 (br s, 1H, NH^+ disappearing in D_2O). Anal. ($C_{13}H_{18}ClNO_2$) C, H, N: C calcd 61.05, found 61.20; H calcd, 7.09, found 6.97; N calcd, 5.48, found 5.52.

5.1.1.7. 2-[(Dimethylamino)methyl]-1-(4-nitrophenyl)-propenone hydrochloride (2g). IR (Nujol, cm^{-1}): 1786. ^{1}H NMR (DMSO-d_6): 2.80 (s, 6H, $(CH_2)_3N$), 4.11 (s,

2H, CH_2), 6.25 (s, 1H, $=CH_2$), 6.88 (s, 1H, $=CH_2$), 8.00 (d, 2H, arom., $J = 9.15$ Hz), 8.36 (d, 2H, arom., $J = 9.15$ Hz), 11.00 (br s, 1H, NH^+ disappearing in D_2O). Anal. ($C_{12}H_{15}ClN_2O_3$) C, H, N: C calcd 53.24, found 53.32; H calcd, 5.58, found 5.64; N calcd, 10.35, found 10.42.

5.1.1.8. 1-(4-Biphenylyl)-2-[(dimethylamino)methyl]-1-propenone hydrochloride (2h). IR (Nujol, cm^{-1}): 1780. ^1H NMR (DMSO-d_6): 2.79 (s, 6H, $(CH_2)_3N$), 4.12 (s, 2H, CH_2), 6.26 (s, 1H, $=CH_2$), 6.75 (s, 1H, $=CH_2$), 7.41–7.96 (m, 9H, arom.), 10.75 (br s, 1H, NH^+ disappearing in D_2O). Anal. ($C_{18}H_{20}ClNO$) C, H, N: C calcd 71.63, found 71.72; H calcd, 6.68, found 6.64; N calcd, 4.64, found 4.62.

5.1.1.9. 2-[(Dimethylamino)methyl]-1-(thiophen-2-yl)-propenone hydrochloride (2i). Mp 150–2 °C. $R_f = 0.13$ ($CHCl_3$–EtOH 9:1). IR (Nujol, cm^{-1}): 1786. ^1H NMR (DMSO-d_6): 2.74 (s, 6H, $(CH_2)_3N$), 4.07 (s, 2H, CH_2), 6.45 (s, 1H, $=CH_2$), 6.66 (s, 1H, $=CH_2$), 7.30 (m, 1H, H_4 thiophene, $J = 3.90$, 4.88 Hz), 7.92 (d, 1H, H_3 thiophene, $J = 3.90$ Hz), 8.15 (d, 1H, H_5 thiophene, $J = 4.88$ Hz) 10.92 (br s, 1H, NH^+ disappearing in D_2O). Anal. ($C_{10}H_{14}ClNOS$) C, H, N: C calcd 51.83, found 51.64; H calcd, 6.09, found 6.16; N calcd, 6.04, found 5.92.

5.1.1.10. 1-(5-Bromothiophen-2-yl)-2-[(dimethylamino)-methyl]-propenone hydrochloride (2j). IR (Nujol, cm^{-1}): 1788. ^1H NMR (DMSO-d_6): 2.72 (s, 6H, $(CH_2)_3N$), 4.03 (s, 2H, CH_2), 6.45 (s, 1H, $=CH_2$), 6.66 (s, 1H, $=CH_2$), 7.46 (d, 1H, H_4 thiophene, $J = 3.90$ Hz), 7.76 (d, 1H, H_3 thiophene, $J = 3.90$ Hz), 11.08 (br s, 1H, NH^+ disappearing in D_2O). Anal. ($C_{10}H_{13}ClBrNOS$) C, H, N: C calcd 38.66, found 38.47; H calcd, 4.22, found 4.30; N calcd, 4.51, found 4.55.

5.1.1.11. 1-(5-Chlorothiophen-2-yl)-2-[(dimethylamino)-methyl]-propenone hydrochloride (2k). IR (Nujol, cm^{-1}): 1783. ^1H NMR (DMSO-d_6): 2.62 (s, 6H, $(CH_2)_3N$), 4.13 (s, 2H, CH_2), 6.40 (s, 1H, $=CH_2$), 6.61 (s, 1H, $=CH_2$), 7.42 (d, 1H, H_4 thiophene, $J = 3.90$ Hz), 7.72 (d, 1H, H_3 thiophene, $J = 3.90$ Hz), 11.08 (br s, 1H, NH^+ disappearing in D_2O). Anal. ($C_{10}H_{13}Cl_2NOS$) C, H, N: C calcd 45.12, found 45.23; H calcd, 4.92, found 5.06; N calcd, 5.26, found 5.18.

5.1.2. General method for synthesis of compounds 1a–k

5.1.2.1. 3-(1H-imidazol-1-yl)-2-[(1H-imidazol-1-yl)-methyl]-1-phenyl-propan-1-one (1a). To 1.0 g (4.4 mmol) of 2-[(dimethylamino)methyl]-1-phenyl-propenone hydrochloride **2a** in 10 ml water–ethanol (8:2), 1.21 g (17.7 mmol) of imidazole was added. The mixture was irradiated in open vial using a domestic Daewoo KOR-63D7 microwave oven at 250 W for a total time of 6 min (2 min for 3 times). Thereafter, the solvent was removed under reduced pressure, the remaining oil was dissolved in 50 ml of $CHCl_3$, and the solution was washed with water until neutrality was achieved. The organic phase was dried over $CaCl_2$ and filtered. The solvent was evaporated in vacuo and the residue was recrystallized from AcOEt to obtain 0.40g (32%) of **1a**. Mp 212–5 °C. $R_f = 0.18$ ($CHCl_3$–EtOH 8:2). IR (Nujol, cm^{-1}): 1784. ^1H NMR (DMSO-d_6): 4.20 (dd, 2H, H_A, upfield H of CH_2; $J_{AB} = 13.91$ Hz, $J_{AX} = 5.86$ Hz), 4.35 (dd, 2H, H_B, downfield H of CH_2; $J_{BA} = 13.91$ Hz, $J_{BX} = 8.05$ Hz), 4.76 (m, 1H, $-CH(CH_2)_2$), 6.79 (s, 2H, $2H_5$ imidazole), 7.12 (s, 2H, $2H_4$ imidazole), 7.40–7.90 (m, 7H, 5H arom., 2H, $2H_2$ imidazole). MS: *m/z* 281 [MH^+]. Anal. ($C_{16}H_{16}N_4O$) C, H, N: C calcd 68.55, found 68.42; H calcd, 5.75, found 5.93; N calcd, 19.99, found 20.12.

Compounds **1b–k** were prepared similarly. Yields and melting points are reported in Table 1.

5.1.2.2. 1-(4-Bromophenyl)-3-(1H-imidazol-1-yl)-2-[(1H-imidazol-1-yl)methyl]-1-pro-pan-1-one (1b). IR (Nujol, cm^{-1}): 1780. ^1H NMR (DMSO-d_6): 4.20 (dd, 2H, H_A, upfield H of CH_2; $J_{AB} = 13.18$ Hz, $J_{AX} = 5.86$ Hz), 4.33 (dd, 2H, H_B, downfield H of CH_2; $J_{BA} = 13.18$ Hz, $J_{BX} = 8.05$ Hz), 4.78 (m, 1H, $-CH(CH_2)_2$), 6.77 (s, 2H, 2 H_5 imidazole), 7.12 (s, 2H, $2H_4$ imidazole), 7.52 (s, 2H, $2H_2$ imidazole), 7.65 (d, 2H, arom., $J = 8.79$ Hz), 7.77 (d, 2H, arom., $J = 8.79$ Hz). MS: *m/z* 359 [MH^+], 361 [MH^++2]. Anal. ($C_{16}H_{15}BrN_4O$) C, H, N: C calcd 53.50, found 53.33; H calcd, 4.21, found 4.34; N calcd, 15.60, found 15.73.

5.1.2.3. 1-(4-Chlorophenyl)-3-(1H-imidazol-1-yl)-2-[(1H-imidazol-1-yl)methyl]-1-pro-pan-1-one (1c). IR (Nujol, cm^{-1}): 1780. ^1H NMR (DMSO-d_6): 4.20 (dd, 2H, H_A, upfield H of CH_2; $J_{AB} = 14.03$ Hz, $J_{AX} = 6.10$ Hz), 4.33 (dd, 2H, H_B, downfield H of CH_2; $J_{BA} = 14.03$ Hz, $J_{BX} = 7.93$ Hz), 4.80 (m, 1H, $-CH(CH_2)_2$), 6.77 (s, 2H, 2 H_5 imidazole), 7.14 (s, 2H, $2H_4$ imidazole), 7.50 (d, 2H, arom., $J = 8.54$ Hz), 7.53 (s, 2H, 2 H_2 imidazole), 7.86 (d, 2H, arom., $J = 8.54$ Hz). MS: *m/z* 315 [MH^+], 317 [MH^++2]. Anal. ($C_{16}H_{15}ClN_4O$) C, H, N: C calcd 61.05, found 61.22; H calcd, 4.80, found 4.88; N calcd, 17.80, found 18.03.

5.1.2.4. 1-(4-Fluorophenyl)-3-(1H-imidazol-1-yl)-2-[(1H-imidazol-1-yl)methyl]-1-pro-pan-1-one (1d). IR (Nujol, cm^{-1}): 1786. ^1H NMR (DMSO-d_6): 4.19 (dd, 2H, H_A, upfield H of CH_2; $J_{AB} = 14.03$ Hz, $J_{AX} = 5.49$ Hz), 4.36 (dd, 2H, H_B, downfield H of CH_2; $J_{BA} = 14.03$ Hz, $J_{BX} = 7.93$ Hz), 4.80 (m, 1H, $-CH(CH_2)_2$), 6.77 (s, 2H, 2 H_5 imidazole), 7.13 (s, 2H, $2H_4$ imidazole), 7.27 (m, 2H, arom.) 7.52 (s, 2H, $2H_2$ imidazole), 7.93 (m, 2H, arom.). MS: *m/z* 299 [MH^+]. Anal. ($C_{16}H_{15}FN_4O$) C, H, N: C calcd 64.42, found 64.21; H calcd, 5.07, found 4.94; N calcd, 18.78, found 18.67.

5.1.2.5. 3-(1H-imidazol-1-yl)-2-[(1H-imidazol-1-yl)-methyl]-1-(4-methylphenyl)-propan-1-one (1e). IR (Nujol, cm^{-1}): 1785. ^1H NMR (DMSO-d_6): 2.32 (s, 3H, CH_3), 4.17 (dd, 2H, H_A, upfield H of CH_2; $J_{AB} = 14.28$ Hz, $J_{AX} = 5.49$ Hz), 4.31 (dd, 2H, H_B, downfield H of CH_2; $J_{BA} = 14.28$ Hz, $J_{BX} = 8.24$ Hz), 4.73 (m, 1H, $-CH(CH_2)_2$), 6.77 (s, 2H, 2 H_5 imidazole), 7.11 (s, 2H, $2H_4$ imidazole), 7.25 (d, 2H, arom., $J = 7.79$ Hz), 7.51 (s, 2H, 2 H_2 imidazole), 7.75 (d, 2H, arom., $J = 7.79$ Hz). MS: *m/z* 295 [MH^+]. Anal. ($C_{17}H_{18}N_4O$)

C, H, N: C calcd 69.37, found 64.21; H calcd, 6.16, found 6.14; N calcd, 19.03, found 19.21.

5.1.2.6. 3-(1H-imidazol-1-yl)-2-[(1H-imidazol-1-yl)methyl]-1-(4-methoxyphenyl)-propan-1-one (1f). IR (Nujol, cm^{-1}): 1781. ^1H NMR (DMSO-d_6): 3.79 (s, 3H, OCH_3), 4.15 (dd, 2H, H_A, upfield H of CH_2; J_{AB} = 13.91 Hz, J_{AX} = 5.12 Hz), 4.32 (dd, 2H, H_B, downfield H of CH_2; J_{BA} = 14.28 Hz, J_{BX} = 8.24 Hz), 4.73 (m, 1H, –C*H*$(CH_2)_2$), 6.76 (s, 2H, 2 H_5 imidazole), 6.92 (d, 2H, arom., J = 8.79 Hz), 7.11 (s, 2H, $2H_4$ imidazole), 7.49 (s, 2H, 2 H_2 imidazole), 7.82 (d, 2H, arom., J = 8.79 Hz). MS: *m/z* 311 [MH^+]. Anal. ($C_{17}H_{18}N_4O_2$) C, H, N: C calcd 65.79, found 65.96; H calcd, 5.85, found 5.90; N calcd, 18.05, found 18.17.

5.1.2.7. 3-(1H-imidazol-1-yl)-2-[(1H-imidazol-1-yl)methyl]-1-(4-nitrophenyl)-propan-1-one (1g). IR (Nujol, cm^{-1}): 1779. ^1H NMR (DMSO-d_6): 3.53 (m,1H, H_x) 3.96 (dd, 1H, upfield H of CH_2; J_{AB} = 10.25 Hz, J_{AX} = 9.50 Hz), 4.06 (dd, 1H, downfield H of CH_2; J_{BA} = 10.25 Hz, J_{BX} = 8.05 Hz) 4.25 (d, 2H, CH2, J = 7.30 Hz), 4.27 (m, 1H, –C*H*$(CH_2)_2$), 6.70 (s, 2H, $2H_5$ imidazole), 7.00 (s, 2H, 2 H_4 imidazole), 7.53 (s, 2H, $2H_2$ imidazole), 7.57 (d, 2H, arom., J = 8.79 Hz), 8.15 (d, 2H, arom., J = 8.79 Hz). MS: *m/z* 326 [MH^+]. Anal. ($C_{16}H_{15}N_5O_3$) C, H, N: C calcd 59.07, found 58.91; H calcd, 4.65, found 4.50; N calcd, 21.53, found 21.66.

5.1.2.8. 1-(4-Biphenylyl)-3-(1H-imidazol-1-yl)-2-[(1H-imidazol-1-yl)methyl]-1-propan-1-one (1h). IR (Nujol, cm^{-1}): 1784. ^1H NMR (DMSO-d_6): 4.22 (dd, 2H, H_A, upfield H of CH_2; J_{AB} = 14.03 Hz, J_{AX} = 5.49 Hz), 4.36 (dd, 2H, H_B, downfield H of CH_2; J_{BA} = 14.03 Hz, J_{BX} = 7.93 Hz), 4.83 (m, 1H, –C*H*$(CH_2)_2$), 6.78 (s, 2H, 2 H_5 imidazole), 7.16 (s, 2H, $2H_4$ imidazole), 7.40–8.00 (m, 11H, 9H arom. and 2H, H_2 imidazole). MS: *m/z* 357 [MH^+]. Anal. calcd for $C_{22}H_{20}N_4O$ (M_W 356.43): C, 74.14; H, 5.66; N, 15.72%; found: C, 74.33; H, 5.54; N, 15.90%.

Anal. ($C_{22}H_{20}N_4O$) C, H, N: C calcd 74.14, found 74.33; H calcd, 5.66, found 5.54; N calcd, 15.72, found 15.90.

5.1.2.9. 3-(1H-imidazol-1-yl)-2-[(1H-imidazol-1-yl)methyl]-1-(thiophen-2-yl)-propan-1-one (1i). Mp 212–5 °C. R_f = 0.25 ($CHCl_3$–EtOH 8:2). IR (Nujol, cm^{-1}): 1788. ^1H NMR (DMSO-d_6): 4.19 (dd, 2H, H_A, upfield H of CH_2; J_{AB} = 14.16 Hz, J_{AX} = 6.35 Hz), 4.32 (dd, 2H, H_B, downfield H of CH_2; J_{BA} = 14.16 Hz, J_{BX} = 8.79 Hz), 4.63 (m, 1H, –C*H*$(CH_2)_2$), 6.77 (s, 2H, 2 H_5 imid.), 7.14 (m, 3H, $2H_4$ imid. and H_4 tiophene), 7.54 (s, 2H, $2H_2$ imid.), 7.93 (d, 1H, H_3 tiophene, J = 3.41 Hz), 8.01 (d, 1H, H_5 tiophene, J = 4.88 Hz). MS: *m/z* 287 [MH^+]. Anal. ($C_{14}H_{14}N_4OS$) C, H, N: C calcd 58.72, found 58.94; H calcd, 4.93, found 5.12; N calcd, 19.57, found 19.38.

5.1.2.10. 1-(5-Bromothiophen-2-yl)-3-(1H-imidazol-1-yl)-2-[(1H-imidazol-1-yl)methyl]-1-propan-1-one (1j). IR (Nujol, cm^{-1}): 1785. ^1H NMR (DMSO-d_6): 4.19 (dd, 2H, H_A, upfield H of CH_2; J_{AB} = 13.18 Hz, J_{AX} = 6.59 Hz), 4.30 (dd, 2H, H_B, downfield H of CH_2; J_{BA} = 13.18 Hz, J_{BX} = 8.24 Hz), 4.61 (m, 1H, –C*H*$(CH_2)_2$), 6.80 (s, 2H, 2 H_5 imidazole), 7.17 (s, 2H, $2H_4$ imidazole), 7.31 (d, 1H, H_4 thiophene, J = 3.67 Hz), 7.56 (s, 2H, $2H_2$ imidazole), 7.77 (d, 1H, H_3 thiophene, J = 3.67 Hz). MS : *m/z* 365 [MH^+], 367 [MH^++2]. Anal. ($C_{14}H_{13}BrN_4OS$) C, H, N: C calcd 46.04, found 46.22; H calcd, 3.59, found 3.69; N calcd, 15.34, found 15.58.

5.1.2.11. 1-(5-Chlorothiophen-2-yl)-3-(1H-imidazol-1-yl)-2-[(1H-imidazol-1-yl)methyl]-1-propan-1-one (1k). IR (Nujol, cm^{-1}): 1787. ^1H NMR (DMSO-d_6): 4.20 (dd, 2H, H_A, upfield H of CH_2; J_{AB} = 14.16 Hz, J_{AX} = 6.35 Hz), 4.32 (dd, 2H, H_B, downfield H of CH_2; J_{BA} = 14.16 Hz, J_{BX} = 8.79 Hz), 4.62 (m, 1H, –C*H*$(CH_2)_2$), 6.80 (s, 2H, 2 H_5 imidazole), 7.17 (s, 2H, $2H_4$ imidazole), 7.22 (d, 1H, H_4 thiophene, J = 3.90 Hz), 7.58 (s, 2H, $2H_2$ imidazole), 7.84 (d, 1H, H_3 thiophene, J = 3.90 Hz). MS : *m/z* 321 [MH^+], 323 [MH^++2]. Anal. ($C_{14}H_{13}ClN_4OS$) C, H, N: C calcd 52.42, found 52.33; H calcd, 4.08, found 4.20; N calcd, 17.46, found 17.68.

5.1.3. General method for synthesis of compounds 1l–m

5.1.3.1. 1-(4-Bromophenyl)-3-(1H-imidazol-1-yl)-2-[(1H-imidazol-1-yl)methyl]-1-propan-1-ol (1l). To a solution of 0.50g (1.39 mmol) of 1-(4-bromophenyl)-3-(1H-imidazol-1-yl)-2-[(1H-imidazol-1-yl)methyl]-propan-1-one **1b** in 20 ml methanol, 0.06g (1.39 mmol) of $NaBH_4$ were added and the reaction mixture was stirred for 3 h at room temperature. Thereafter, the solvent was completely evaporated under reduced pressure, the obtained oil was dissolved in 10 ml of $CHCl_3$ and the solution was washed with cold water until neutrality. The organic phase was dried ($CaCl_2$) and filtered. The filtrate was evaporated to dryness to give a residue which was re-crystallized from dichloromethane to give 0.15 g (30%) of **1l**. Mp 180–2 °C. R_f = 0.26 ($CHCl_3$–EtOH 8:2). IR (Nujol, cm^{-1}): 3130. ^1H NMR (DMSO-d_6): 3.71 (dd, 2H, H_A, upfield H of CH_2; J_{AB} = 13.91 Hz, J_{AX} = 5.86 Hz), 3.85 (m, 1H, H_x, –C*H*$(CH_2)_2$),4.08 (dd, 2H, H_B, downfield H of CH_2; J_{BA} = 13.91 Hz, J_{BX} = 8.05 Hz), 4.20 (m, 1H, *CH*OH), 5.77 (d, 1H, OH, J = 4.02 Hz, disappearing in D_2O), 6.69–7.64 (m, 10H, arom. and imidazole). MS: *m/z* 361 [MH^+], 363 [MH^+ + 2]. Anal. ($C_{16}H_{17}BrN_4O$) C, H, N: C calcd 53.20, found 52.98; H calcd, 4.74, found 4.62; N calcd, 15.51, found 15.39.

Compound **1m** was prepared similarly. Yield and melting point are reported in Table 1.

5.1.3.2. 3-(1H-imidazol-1-yl)-2-[(1H-imidazol-1-yl)-methyl]-1-(4-metoxyphenyl)-propan-1-ol (1m). IR (Nujol, cm^{-1}): 3144. ^1H NMR (DMSO-d_6): 3.68 (dd, 2H, H_A, upfield H of CH_2; J_{AB} = 13.42 Hz, J_{AX} = 6.10 Hz), 3.73 (m, 3H, OCH_3), 3.88 (m, 1H, H_x, –C*H*$(CH_2)_2$),4.05 (dd, 2H, H_B, downfield H of CH_2; J_{BA} = 13.42 Hz, J_{BX} = 7.93. Hz), 4.36 (m, 1H, *CH*OH), 5.80 (d, 1H, OH, J = 4.20 Hz, disappearing in D_2O), 6.80–7.60 (m, 10H, arom. and imidazole). MS: *m/z* 313 [MH^+]. Anal.

($C_{17}H_{20}N_4O_2$) C, H, N: C calcd 65.37, found 65.21; H calcd, 6.45, found 6.34; N calcd, 17.94, found 18.07.

5.2. Microbiology

Two clinical isolates of *Candida species*, *C. glabrata* 123 and *C. albicans* 3038, were selected for testing the antifungal activity of the title compounds.

The susceptibility of the *Candida* spp. isolates to the newly synthesized compounds was determined measuring MIC by a microdilution RPMI reference method, according to the recommendations of the National Committee for Clinical Laboratory Standards (NCCLS, 1997). Stock solutions of chemicals were prepared in DMSO at a concentration of 4 mg/mL; miconazole and amphotericin B were used as reference test compounds. Each MIC was determined twice in duplicate experiments after 24 and 48 h incubation time, respectively. The in vitro antitubercular activity was evaluated measuring MIC by MRA, a microdilution resazurin assay performed in liquid medium within 8 days of incubation on *M. tuberculosis* H37Rv.[25] Briefly, twofold dilutions of each compound were prepared from stock solutions in 96-well plates in complete 7H9 broth, final compound concentrations being 128–0.125 μg/mL. Twenty microliters of each bacterial suspension was added to 180 μL of drug-containing culture medium. The plates were sealed and incubated for 7 days at 37 °C; 5 μL of esazurin (Sigma-Aldrich, 10 mg/mL sterile water stock solution) was added per well, coloring blue; plates were allowed to incubate at 37 °C for additional 24 h. Plates were finally read by visual inspection for color change from blue to pink in wells containing live *Mycobacteria*. MIC was defined as the lowest drug concentration that prevented resazurin color change; MIC was determined twice in duplicate experiments and was considered bactericidal by viable counts from blue wells when 99% cfu was inhibited. Rifampicin was always included as positive control in each experiment; DMSO was also evaluated and was always devoid of inhibiting activity up to the concentration of 2% (v/v).

5.3. Molecular modeling

All calculations were carried out on a cluster of Silicon Graphics Octane R12K computers and were based on a series of well-validated procedures.[8,20] The starting point of all simulations was our high quality homology model of the cytochrome P450 sterol 14α-demethylase (14DM) from *C. albicans*.[8] All inhibitor molecules (plus miconazole and fluconazole, used as reference compounds, see Results and discussion) were generated using the Biopolymer module of InsightII[26] energy minimized using the *Sander* module of the AMBER 7.0 suite of programs,[27,28] with the *Parm94* version[29] of the AMBER force field (FF), and a convergence criterion equal to 10^{-4} kcal/(mol Å). A conformational search was carried out using a combined molecular mechanics/molecular dynamics simulated annealing (MDSA) protocol (i.e., five repeated temperature cycles—from 300 to 1000 K and back—in the constant volume/constant temperature ensemble, followed by energy minimization, again using 10^{-4} kcal/(mol Å) as a convergence criterion).[19,30–33]For each compound **1a**–**m**, only the structures corresponding to the minimum energy were selected for further modeling. The atomic partial charges for the geometrically optimized compounds were obtained via the RESP protocol ,[24,34] producing the electrostatic potentials by single-point quantum mechanical calculations at the Hartree–Fock level with a 6–31G* basis set, using the Merz–Singh–Kollman van der Waals parameters.[35,36]

The optimized structures of the antifungal molecules were docked into the 14DM active site according to a procedure already successfully employed for this enzyme and similar compounds.[8,20] Accordingly, it will only briefly described below. The software AutoDock 3.0[37] was employed to estimate the possible binding orientations of all compounds in the receptor. This popular program performs automated docking of flexible ligands to a receptor by rapid energy evaluation achieved by precalculating atomic affinity potentials for each atom type. The protocol employed in this work[8,20] was based on the following settings: (i) grids were extended 60 Å from the enzyme binding site; (ii) a grid spacing of 0.375 Å and 120 grid points were applied in each Cartesian direction so as to calculate mass-centered grid maps; (iii) AMBER 12–6 and 12–10 Lennard-Jones parameters were used in modeling van der Waals interactions and hydrogen bonding (N–H, O–H, and S–H), respectively. In the generation of the electrostatic grid maps, the distance-dependent relative permittivity of Mehler and Solmajer[37] was applied. For the docking of each compound to the protein, three hundred Monte Carlo/Simulated Annealing (MC/SA) runs were performed, with 100 constant temperature cycles for simulated annealing. For these calculations, the GB/SA implicit water model[38,39] was used to mimic a solvated environment. The rotation of the angles ϕ and φ, and the angles of side chains were set free during the calculations. All other parameters of the MC/SA algorithm were kept as default. Following the docking procedure, all structures of compounds **1a**–**m** were subjected to cluster analysis with a tolerance of 1 Å for an all-atom root-mean-square (RMS) deviation from a lower-energy structure representing each cluster family. In the absence of any relevant crystallographic information, the structure of each resulting complex characterized by the lowest interaction energy was selected for further evaluation.

Each best substrate/14DM complex resulting from the automated docking procedure was further refined in the AMBER suite using the quenched molecular dynamics method (QMD).[40–42] In this case, 100 ps MD simulation at 300 K was employed to sample the conformational space of the substrate–enzyme complex in the GB/SA continuum solvation environment.[38,39] The integration step was equal to 1 fs. After each picosecond, the system was cooled to 0 K, the structure was extensively minimized and stored. To prevent global conformational changes of the enzyme, the backbone of the protein binding site was constrained by a harmonic force constant of 100 kcal/Å, whereas the amino acid

side chains and the ligands were allowed move without any constraint.

The best energy configuration of each complex resulting from the previous step was solvated by adding a sphere of TIP3P water molecules [43] with a 3 nm radius from the mass center of the ligand with the use of the cap option of the *Leap* module of AMBER 7.0 The protein complex was neutralized adding a suitable number of counterions (Na^+ and Cl^-) in the positions of largest electrostatic potential, as determined by the module *Cion* of the AMBER platform. The counterions having distances larger than 25 Å from the active site were fixed in space during all simulations to avoid artifactual long-range electrostatic effects on the calculated free energies. After energy minimization of the water molecules for 1500 steps, and MD equilibration of the water sphere with fixed solute for 20 ps, further unfavorable interactions within the structures were relieved by progressively smaller positional restraints on the solute (from 25 to 0 kcal/(mol Å^2)) for a total of 4000 steps. Each system was gradually heated to 300 K in three intervals, allowing a 5 ps interval per each 100 K, and then equilibrated for 50 ps at 300 K, followed by 400 ps of data collection runs, necessary for the estimation of the free energy of binding (vide infra). After the first 20 ps of MD equilibration, additional TIP3P water molecules were added to the 3 nm water cap to compensate for those who were able to diffuse into gaps of the enzyme. The MD simulations were performed at 300 K using the *Parm94* FF[29] with the heme model parameters of Paulsen and Ornstein,[44] the Berendsen coupling algorithm,[45] an integration time step of 2 fs, and the applications of the SHAKE algorithm[46] to constrain all bonds to their equilibrium values, thus removing high frequency vibrations. Long-range nonbonded interactions were truncated by using a 30 Å residue-based cut-off.

For the calculation of the binding free energy between 14DM and all inhibitors in water, a total of 400 snapshots were saved during the MD data collection period described above, one snapshot per each 1 ps of MD simulation.

The binding free energy ΔG_{BIND} of each complex in water was estimated via the widely used MM/PBSA (Molecular Mechanics/Poisson–Boltzmann Surface Area) methodology, originally proposed by Peter Kollman and coworkers.[9] According to this approach, ΔG_{BIND} can be calculated from computational analysis of a single simulation of each ligand-bound protein, and includes explicit computed components corresponding to 'gas-phase' protein/ligand interactions (ΔE_{MM}), conformational entropy ($T\Delta S$), and solvation contributions (ΔG_{SOLV}):

$$\Delta G_{\mathrm{BIND}} = \Delta E_{\mathrm{MM}} + \Delta G_{\mathrm{SOLV}} - T\Delta S \qquad (1)$$

The term ΔE_{MM} in Eq. 1 can be further split into contributions from electrostatic ($\Delta E^{\mathrm{MM}}_{\mathrm{ELE}}$) and van der Waals ($\Delta E^{\mathrm{MM}}_{\mathrm{vDW}}$) energies:

$$\Delta E_{\mathrm{MM}} = \Delta E^{\mathrm{MM}}_{\mathrm{ELE}} + \Delta E^{\mathrm{MM}}_{\mathrm{vdW}} \qquad (2)$$

The solvation free energy, ΔG_{SOLV}, can in turn be expressed as the sum of an electrostatic component, $\Delta G^{\mathrm{SOLV}}_{\mathrm{ELE}}$, and a nonpolar contribution, $\Delta G^{\mathrm{SOLV}}_{\mathrm{NP}}$:

$$\Delta G_{\mathrm{SOLV}} = \Delta G^{\mathrm{SOLV}}_{\mathrm{ELE}} + \Delta G^{\mathrm{SOLV}}_{\mathrm{NP}} \qquad (3)$$

$\Delta G^{\mathrm{SOLV}}_{\mathrm{ELE}}$ was calculated by solving the finite-difference Poisson–Boltzmann equation using the *Delphi* package,[47] with the Parse atomic radii,[48] and Cornell et al. charges,[29] with interior and exterior dielectric constants equal to 1 and 80, respectively. A grid spacing of 2/Å, extending 20% beyond the dimensions of the solute, was employed. The nonpolar component in Eq. 3 was obtained from the solvent accessible surface area (SASA) using the following relationship[48]: $\Delta G^{\mathrm{SOLV}}_{\mathrm{NP}} = \gamma \mathrm{SASA} + \beta$, in which $\gamma = 0.00542$ kcal/(mol Å^2), $\beta = 0.92$ kcal/mol, and the surface area evaluated by means of the MSMS software.[11]

Different approaches are available to estimate the configurational/conformational entropy component $T\Delta S$ in Eq. 1.[49–52] Considering that normal mode has been successfully applied in estimating the binding entropy for several biological systems,[53] including the same enzyme and structurally related compounds,[8,20] this method was the one selected in this work to evaluate $T\Delta S$ values. In the first step of this calculation, an 8 Å sphere around the ligand was cut out from an MD snapshot for each ligand–protein complex. This value was shown to be large enough to yield converged mean changes in solute entropy. On the basis of the size-reduced snapshots of the complex, we generated structures of the uncomplexed reactants by removing the atoms of the protein and ligand, respectively. Each of those structures was minimized, using a distance dependent dielectric constant $\varepsilon = 4r$, to account for solvent screening, and its entropy was calculated using classical statistical formulas and normal mode analysis. To minimize the effects due to different conformations adopted by individual snapshots we averaged the estimation of entropy over 10 snapshots.

Acknowledgment

This research was carried out with the financial support of the Italian M.U.R.S.T. (60%) (University of Trieste 2001).

References and notes

1. Bellamine, A.; Mangla, A. T.; Nes, W. D.; Watermann, M. R. *Proc. Natl. Acad. Sci. U.S.A.* **1999**, *96*, 8937.
2. Morris, S.; Bai, G. H.; Suffys, P.; Portilo-Gomez, L.; Fairchok, M.; Rouse, D. *J. Infect. Dis.* **1995**, *171*, 954.
3. Guardiola-Diaz, H. M.; Foster, L. A.; Mushrush, D.; Vaz, A. D. N. *Biochem. Pharmacol.* **2001**, *61*, 1463.
4. Zhang, W.; Ramamoorthy, Y.; Kilicarslan, T.; Nolte, H.; Tendale, R. F.; Sellers, E. M. *Drug Metab. Dispos.* **2002**, *30*, 314.
5. Telzak, E. E.; Sepkowitz, K.; Alpert, P.; Mannheimer, S.; Mederd, F.; El-Sadr, W.; Blum, S.; Gagliardi, A.; Salomon, N.; Turett, G. *N. Engl. J. Med.* **1995**, *333*, 907.

6. Basso, L. A.; Blanchard, J. S. *Adv. Exp. Med. Biol.* **1998**, *456*, 115.
7. Bastian, I.; Colebuuders, R. *Drugs* **1999**, *58*, 633.
8. Banfi, E.; Scialino, G.; Zampieri, D.; Mamolo, M. G.; Vio, L.; Ferrone, M.; Fermeglia, M.; Paneni, M. S.; Pricl, S. *J. Antimicrob. Chemother.* **2006**, *58*, 76.
9. Srinivasan, J.; Cheatham, T. E., III; Cieplak, P.; Kollman, P. A.; Case, D. A. *J. Am. Chem. Soc.* **1998**, *120*, 9401.
10. Honig, B.; Nicholls, A. *Science* **1995**, *268*, 1144.
11. Sanner, M. F.; Olson, A. J.; Spehner, J. C. *Biopolymers* **1996**, *38*, 305.
12. (a) Ulbrich, H.; Priewe, H.; Schröder, E. *Eur. J. Med. Chem.* **1976**, *11*, 343; (b) Lesieur, I.; Lesieur, D.; Lespagnol, C.; Cazin, M.; Brunet, C.; Luyckx, M.; Mallevais, M. L.; Delacourte, A.; Dubreuil, L.; Devos, L.; Romond, C. *Arzneim. Forsch.* **1986**, *36*, 20; (c) Traxler, P.; Trinks, U.; Buchdunger, E.; Mett, H.; Meyer, T.; Müller, M.; Regenass, U.; Rösel, J.; Lydon, N. *J. Med. Chem.* **1995**, *38*, 2441.
13. Girreser, V.; Heber, D.; Shvett, M. *Synthesis* **1998**, *5*, 715.
14. Ogata, M.; Matsumoto, H.; Kida, S.; Shimizu, S.; Tawara, K.; Kawamura, Y. *J. Med. Chem.* **1987**, *30*, 1497.
15. Fioravanti, R.; Biava, M.; Porretta, G. C.; Artico, M.; Lampis, G.; Deidda, D.; Pompei, R. *Med. Chem. Res.* **1997**, *7*, 87.
16. Biava, M.; Fioravanti, R.; Porretta, G. C.; Sleiter, G.; Ettorre, A.; Deidda, D.; Lampis, G.; Pompei, R. *Med. Chem. Res.* **1997**, *7*, 228.
17. Mamolo, M. G.; Zampieri, D.; Falagiani, V.; Vio, L.; Fermeglia, M.; Ferrone, M.; Pricl, S.; Banfi, E.; Scialino, G. *ARKIVOC* **2004**, *5*, 231.
18. Podust, L. M.; Poulos, T. L.; Waterman, M. R. *Proc. Natl. Acad. Sci. U.S.A.* **2001**, *98*, 3068.
19. Manfredini, S.; Angusti, A.; Ciliberti, N.; Durini, E.; Vertuani, S.; Buzzoni, L.; Coslanich, A.; Fermeglia, M.; Ferrone, M.; Paneni, M. S.; Pricl, S.; La Colla, P.; Sanna, G.; Cadeddu, A.; Mura, M.; Loddo, R. In *Framing the Knowledge of Viral Hepatitis*; Schinazi, R. F., Schiff, E., Eds.; IHL Press: Arlington, MA, USA, 2005; pp 279–318.
20. Mamolo, M. G.; Zampieri, D.; Vio, L.; Fermeglia, M.; Ferrone, M.; Pricl, S.; Scialino, G.; Banfi, E. *Bioorg. Med. Chem.* **2005**, *13*, 3797.
21. Darden, T.; York, D.; Pedersen, L. *J. Chem. Phys.* **1993**, *98*, 10089.
22. Raag, R.; Li, H.; Jones, B. C.; Poulos, T. L. *Biochemistry* **1993**, *32*, 4571.
23. Radmer, R. J.; Kollman, P. A. *J. Comput.-Aided Mol. Des.* **1998**, *12*, 215.
24. Bayly, C. I.; Cieplak, P.; Cornell, W. D.; Kollman, P. A. *J. Phys. Chem.* **1993**, *97*, 10269.
25. Banfi, E.; Scialino, G.; Monti-Bragadin, C. *J. Antimicrob. Chemother.* **2003**, *52*, 796.
26. Insight II Program Package (2000.1), Accelrys Inc., San Diego, CA, USA.
27. Case, D. A.; Pearlman, D. A.; Caldwell, J. W.; Cheatham, T. E., III; Ross, W. S.; Simmerling, C. L.; Darden, T. A.; Merz, K. M.; Stanton, R. V.; Cheng, A. L.; Vincent, J. J.; Crowley, M.; Tsui, V.; Radmer, R. J.; Duan, Y.; Pitera, J.; Massova, I.; Seibel, G. L.; Singh, U. C.; Weiner, P. K.; Kollman, P. A. *AMBER 6*; University of California: San Francisco, USA, 1999.
28. Pearlman, D. A.; Case, D. A.; Caldwell, J. W.; Ross, W. S., III; Cheatham, T. E., III; DeBolt, S.; Ferguson, D.; Seibel, G. L.; Kollman, P. A. *Comput. Phys. Commun.* **1995**, *91*, 1.
29. Cornell, W. D.; Cieplak, P.; Bayly, C. I.; Gould, I. R.; Merz, K. M., Jr.; Ferguson, D. M.; Spellmeyer, D. C.; Fox, T.; Caldwell, J. W.; Kollman, P. A. *J. Am. Chem. Soc.* **1995**, *117*, 5179.
30. Fermeglia, M.; Ferrone, M.; Pricl, S. *Bioorg. Med. Chem.* **2002**, *10*, 2471.
31. Felluga, F.; Pitacco, G.; Valentin, E.; Coslanich, A.; Fermeglia, M.; Ferrone, M.; Pricl, S. *Tetrahedron: Asymmetry* **2003**, *14*, 3385.
32. Manfredini, S.; Solaroli, N.; Angusti, A.; Nalin, F.; Durini, E.; Vertuani, S.; Pricl, S.; Ferrone, M.; Spadari, S.; Focher, F.; Verri, A.; De Clercq, E.; Balzarini, E. *J. Antivir. Chem. Chemother.* **2003**, *14*, 183.
33. Di Santo, R.; Fermeglia, M.; Ferrone, M.; Paneni, M. S.; Costi, R.; Artico, M.; Roux, A.; Gabriele, M.; Tardiff, K. D.; Siddiqui, A.; Pricl, S. *J. Med. Chem.* **2005**, *48*, 6304.
34. Fox, T.; Kollman, P. A. *J. Phys. Chem. B* **1998**, *102*, 8070.
35. Besler, B. H.; Merz, K. M.; Kollman, P. A. *J. Comput. Chem.* **1990**, *11*, 431.
36. Singh, U. C.; Kollman, P. A. *J. Comput. Chem.* **1984**, *5*, 129.
37. Mehler, E. L.; Solmajer, T. *Protein Eng.* **1991**, *4*, 903.
38. Jayaram, B.; Sprous, D.; Beveridge, D. L. *J. Phys. Chem. B* **1998**, *102*, 9571.
39. Weiser, J.; Shenkin, P. S.; Still, W. C. *J. Comp. Chem.* **1999**, *20*, 217.
40. Felluga, F.; Fermeglia, M.; Ferrone, M.; Pitacco, G.; Pricl, S.; Valentin, E. *Tetrahedron: Asymmetry* **2002**, *13*, 475.
41. Frecer, V.; Kabelac, M.; De Nardi, P.; Pricl, S.; Miertus, S. J. *J. Mol. Graph. Model* **2004**, *22*, 209.
42. Metullio, L.; Ferrone, M.; Coslanich, A.; Fuchs, S.; Fermeglia, M.; Paneni, M. S.; Pricl, S. *Biomacromolecules* **2004**, *5*, 1371.
43. Jorgensen, W. L.; Chandrasekhar, J.; Madura, J. D.; Impey, R. W.; Klein, M. L. *J. Comput. Phys.* **1983**, *79*, 926.
44. Paulsen, M. D.; Ornstein, R. L. *Proteins: Struct. Funct. Genet.* **1991**, *11*, 184.
45. Berendsen, H. J. C.; Postma, J. P. M.; van Gunsteren, W. F.; DiNola, A.; Haak, J. R. *J.Comput. Phys.* **1984**, *81*, 3684.
46. Ryckaert, J. P.; Ciccotti, G.; Berendsen, H. J. C. *J. Comput. Phys.* **1977**, *23*, 327.
47. Gilson, M. K.; Sharp, K. A.; Honig, B. H. *J. Comput. Chem.* **1987**, *9*, 327.
48. Sitkoff, D.; Sharp, K. A.; Honig, B. H. *J. Phys. Chem.* **1994**, *98*, 1978.
49. Wilson, E. B.; Decius, J. C.; Cross, P. C. *Molecular Vibrations*; McGraw-Hill: New York, 1955.
50. Brooks, B. R.; Janežič, D.; Karplus, M. *J. Comput. Chem.* **1995**, *16*, 1522.
51. Janežič, D.; Brooks, B. R. *J. Comput. Chem.* **1995**, *16*, 1543.
52. Roccatano, D.; Amadei, A.; Apol, M. E. F.; Nola, A. D.; Berendsen, H. J. C. *J. Chem. Phys.* **1998**, *109*, 6358.
53. See for instance: (a) Chong, L. T.; Duan, Y.; Wang, I.; Massova, I.; Kollman, P. *Proc. Natl. Acad. Sci. U.S.A.* **1999**, *96*, 14330; (b) Massova, I.; Kollman, P. A. *J. Am. Chem. Soc.* **1999**, *121*, 8133; (c) Wang, J.; Morin, P.; Wang, W.; Kollman, P. A. *J. Am. Chem. Soc.* **2001**, *123*, 5221; (d) Minehardt, T. J.; Marzari, N.; Cooke, R.; Pate, E.; Kollman, P. A.; Car, R. *Biophys. J.* **2002**, *82*, 660; (e) Gouda, H.; Kuntz, I. D.; Case, D. A.; Kollman, P. A. *Biopolymers* **2003**, *68*, 16; (f) Ferrone, M.; Perrone, F.; Tamborini, E.; Paneni, M. S.; Fermeglia, M.; Suardi, S.; Pastore, E.; Delia, D.; Pierotti, M. A.; Pricl, S.; Pilotti, S. *Mol. Cancer Ther.* **2006**, *5*, 1467; (g) Tamborini, E.; Pricl, S.; Negri, T.; Lagonigro, M. S.; Piselli, F.; Greco, A.; Gronchi, A.; Casali, P. G.; Ferrone, M.; Fermeglia, M.; Carbone, A.; Pierotti, M. A.; Pilotti, S. *Oncogene* **2006**, *25*, 6140; (h) Pricl, S.; Fermeglia, M.; Ferrone, M.; Tamborini, E. *Mol. Cancer Ther.* **2005**, *4*, 1167.